Nanoelectronics and Its New Materials – A NEW ERA OF NANOSCIENCE

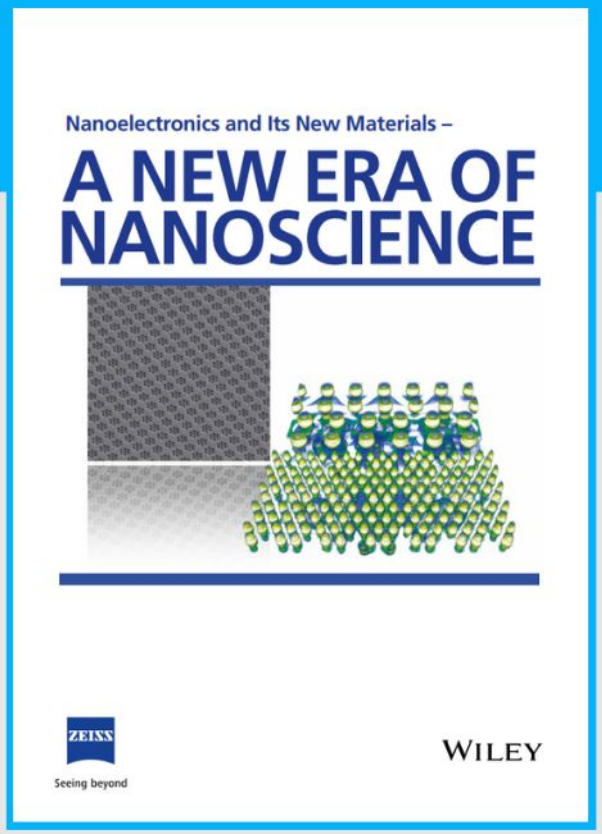

Discover the recent advances in electronics research and fundamental nanoscience.

Nanotechnology has become the driving force behind breakthroughs in engineering, materials science, physics, chemistry, and biological sciences. In this compendium, we delve into a wide range of novel applications that highlight recent advances in electronics research and fundamental nanoscience. From surface analysis and defect detection to tailored optical functionality and transparent nanowire electrodes, this eBook covers key topics that will revolutionize the future of electronics.

To get your hands on this valuable resource and unleash the power of nanotechnology, simply download the eBook now. Stay ahead of the curve and embrace the future of electronics with nanoscience as your guide.

ZEISS

Seeing beyond

WILEY

NANO · MICRO small
www.small-journal.com

Biosynthesis of Multifunctional Transformable Peptides for Inducing Tumor Cell Apoptosis

Yufei Di, Qi Shen, Zhiwen Yang, Gang Song, Tiantian Fang, Yazhou Liu, Yamei Liu, Qun Luo, Fuyi Wang, Xuehai Yan, Haotian Bai, Yiming Huang, Fengting Lv, and Shu Wang**

Engineered nanomaterials hold great promise to improve the specificity of disease treatment. Herein, a fully protein-based material is obtained from nonpathogenic *Escherichia coli* (*E. coli*), which is capable of morphological transformation from globular to fibrous in situ for inducing tumor cell apoptosis. The protein-based material P1 is comprised of a β-sheet-forming peptide KLVFF, pro-apoptotic protein BAK, and GFP along with targeting moieties. The self-assembled nanoparticles of P1 transform into nanofibers in situ in the presence of cathepsin B, and the generated nanofibrils favor the dimerization of functional BH3 domain of BAK on the mitochondrial outer membrane, leading to efficient anticancer activity both in vitro and in vivo via mitochondria-dependent apoptosis through Bcl-2 pathway. To precisely manipulate the morphological transformation of biosynthetic molecules in living cells, a spatiotemporally controllable anticancer system is constructed by coating P1-expressing *E. coli* with cationic conjugated polyelectrolytes to release the peptides in situ under light irradiation. The biosynthetic peptide-based enzyme-catalytic transformation strategy in vivo would offer a novel perspective for targeted delivery and shows great potential in precision disease therapeutics.

1. Introduction

Peptide-based materials (PBMs) are a class of attractive biomaterials with excellent biodegradability, high biocompatibility, and well-modified structures.[1] Benefiting from the rapid development of chemistry and biology, PBMs are endowed with various functions for different application scenarios like tissue engineering, drug delivery, and bioimaging.[2] As the substructure of proteins, peptides also display the potential to form higher order structures via the self-assembly mediated by hydrophobic, electrostatic, and hydrogen-bond interactions,[3] which are endowed with well-controllable assembly properties and superior bio-functions. Controllable self-assembly of PBMs in living cells triggered by enzyme,[4] reactive oxygen species (ROS),[5] pH,[6] and light[7] allows for the creation of peptide nanostructures with broad functions ranging from disease diagnostics to therapeutics. However, most in vivo transformable peptide-based materials presently utilize chemically synthetic methods requiring multi-step reactions, which are time-consuming and uneconomic because of the sophisticated separation and purification processes. Moreover, it is difficult to chemically synthesize long peptides with biological activities.

Living bacteria have been employed to treat a broad variety of cancers. Bacterial and mammalian cells can be engineered to complete the biosynthesis of PBMs. The advantages of biosynthesis include better biocompatibility and biosafety, as well as reduced production time and cost.[8] In addition, the facile editability of biosynthesis endows more possibility to this technique, where the various functions could be integrated by adding a corresponding sequence into the DNA of the plasmid.[9] For instance, Wang and co-workers reported nano-vaccines which consist of self-assembled proteinaceous nanoparticles and could act as an immunostimulant against tumors.[10] Despite all the advantages of the biosynthesis of PBMs, precisely manipulating the morphology transformation of biosynthesized PBMs in living cells with regulated functions remains challenging because of the complexity of the intracellular environment.

Y. Di, Q. Shen, Z. Yang, G. Song, H. Bai, Y. Huang, F. Lv, S. Wang
Beijing National Laboratory for Molecular Sciences
Key Laboratory of Organic Solids
Institute of Chemistry
Chinese Academy of Sciences
Beijing 100190, P. R. China
E-mail: lvft@iccas.ac.cn; wangshu@iccas.ac.cn

Y. Di, Z. Yang, G. Song, Q. Luo, F. Wang, S. Wang
College of Chemistry
University of Chinese Academy of Sciences
Beijing 100049, P. R. China

T. Fang, Q. Luo, F. Wang
Key Laboratory of Analytical Chemistry for Living Biosystems
Institute of Chemistry
Chinese Academy of Sciences
Beijing 100190, P. R. China

Y. Liu, Y. Liu, X. Yan
State Key Laboratory of Biochemical Engineering
Institute of Process Engineering
Chinese Academy of Sciences
Beijing 100190, P. R. China

The ORCID identification number(s) for the author(s) of this article can be found under https://doi.org/10.1002/smll.202303035

DOI: 10.1002/smll.202303035

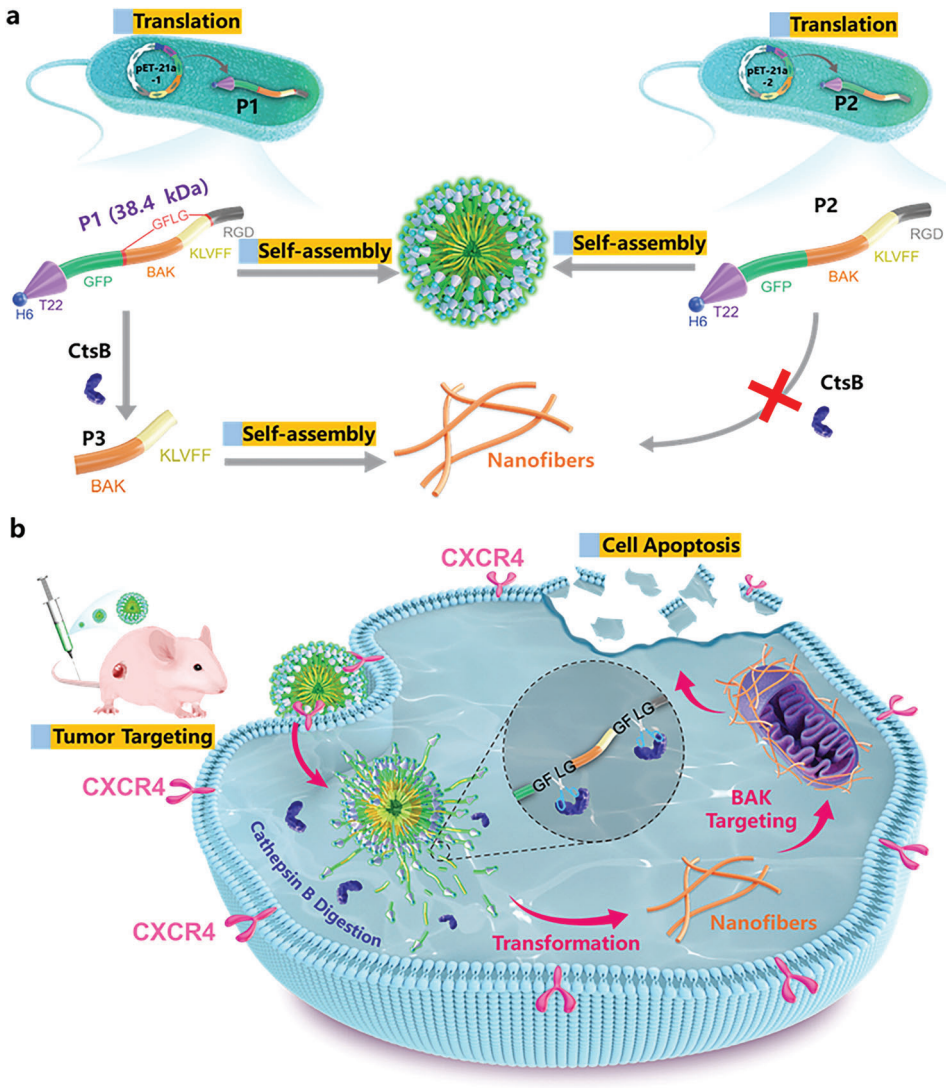

Figure 1. a) Schematic illustration of the modular design, expression, and self-assembly behavior of the recombinant protein P1, and the enzyme catalytic morphology transformation strategy to form nanofibrous structures. For the control peptide P2 without GFLG units, there is no conformational change after the treatment of CtsB. b) Morphology transformation of P1 by CtsB enzyme catalysis to form nanofibrous structures for inducing tumor cell apoptosis in the mouse model.

In this study, we report a biosynthetic peptide-based material, P1, which possesses the ability to transform from globular to fibrous morphology in situ for inducing tumor cell apoptosis (**Figure 1**). This enzyme-catalytic transformable recombinant protein H6-T22-GFP-BAK-KLVFF-RGD was designed to integrate multiple functions. The 6× His tag would facilitate purification and detection in cells with antibody-based methods. GFP and T22 would function as the tracker of nanoparticles and targeting moieties that could target CXCR4$^+$ cancer cells.[11] The BAK motif was introduced to induce tumor cell apoptosis.[12] As a member of the Beclin-2 family, BAK is the only pro-apoptotic protein localized on the mitochondrial outer membrane (MOM).[13] The functional BH3 domain of BAK could oligomerize at the mitochondrial, the exposure of which is considered a key step in apoptosis, leading to dimerization and the release of cytochrome C and other proapoptotic factors from mitochondria.[14] Therefore, a hydrophilic peptide was incorporated to envelop BH3 to reduce its pro-apoptotic activity, which could facilitate P1 to reorganize into β-sheet fibrous structures to expose the BH3 due to the shedding of the hydrophilic green fluorescent protein shell. A hydrogen-bonding peptide KLVFF would work as the scaffold for the formation of β-sheet structured fibers with targeting peptide RGD terminal. The RGD peptide would enhance the targeting of the integrin $\alpha_v\beta_3$ over-expressing tumor cells. Enzyme-cleavable peptide GFLG was placed at opposite ends of BAK-KLVFF.[5a,15] Meanwhile, the control peptide P2 without enzyme-cleavable site GFLG was biosynthesized by similar methods. Another peptide P3 was the enzyme digestion product of P1 and was prepared by standard solid-phase peptide synthesis. Due to the overall balance of hydrophilic GFP peptide and hydrophobic organizing sequence, P1 could self-assemble into nanoparticles, which could target the tumor site and internalize into the

cells. Cathepsin B (CtsB) is a significant lysosomal protease overexpressed in various tumors.[16] The presence of the CtsB enzyme cleavage sites allows the P1 shed the hydrophilic GFP shell in tumor cells, which makes the nanoparticles transform into nanofibers to expose their active site (BH3 domain). Besides, the generation of nanofibrils is more favorable for its dimerization on MOM. Finally, the nanofibers localized to the MOM and aggregated to mediate the membrane permeabilization leading to the release of cytochrome C, resulting in efficient inhibition of tumor growth. Compared to other peptide-based materials, the engineered PBM exhibited great biocompatibility and capability of organelle-located morphological transformation with enhanced biological functions. In addition, a spatiotemporally controllable anticancer system was constructed by coating P1-expressing *Escherichia coli* (*E. coli*) with cationic conjugated polyelectrolytes to release the peptides in situ.

2. Results and Discussion

Isopropyl-beta-D-thiogalactopyranoside induced *E. coli* transformed with the plasmid of pET21a-His-T22-GFP-BAK-KLVFF-RGD were lysed and the recombinant protein was subsequently purified using Ni-NTA affinity chromatography to purify the 6× His-tagged protein products. The proteins were confirmed by the sodium dodecyl sulfate-polyacrylamide gel electrophoresis (SDS-PAGE) and western blotting analysis, and coomassie blue staining showed that fusion monomers were the expected 38.44 kDa in size (**Figure 2**a), which was consistent with the mass spectrum results of P1 (Figure S1, Supporting Information). The purified peptide P1 exhibited the characteristic fluorescence of GFP with an emission maximum at 520 nm, as depicted in Figure S2, Supporting Information. The successful expression of P1 by bacteria was verified, and the probable structure of this peptide was investigated by molecular modeling. As shown in Figure S3, Supporting Information, the iterative threading assembly refinement (I-TASSER) model showed a cylindric GFP extending a positive charge of the T22 peptide.[17] Meanwhile, the mass spectrum and SDS-PAGE assessment of the control peptide P2 were performed and shown in Figure S4, Supporting Information.

The molecular transformation of P1 incubated with CtsB was investigated with high-performance liquid chromatography-MS. A new peak corresponding to P3 in LC-MS (Figure 2b) verified that P1 was cleaved by CtsB at the designed digestion site GFLG. To investigate the conformational change of P1 assemblies, transmission electron microscopy (TEM) and circular dichroism (CD) spectra were performed. As evidenced in Figure 2d, P1 formed nanoparticles about 20 nm in diameter, which was consistent with the dynamic light scattering result of 22.2 ± 2.3 nm (Figure S5, Supporting Information). The self-assembly of P1 appeared concentration dependent. At 500 μg mL^{-1}, P1 formed a spherical morphology as observed by TEM (Figure S6, Supporting Information). At concentration of 50 μg mL^{-1} or lower, the morphology of P1 became sparse and irregular due to a significant reduction in concentration. The formation of the spherical shape of the engineered PBM was realized by the hydrophilic GFP and the other hydrophobic amino acids, which could self-assemble into a spherical shape due to hydrophilic and hydrophobic interactions.[18] The morphology did not change from spherical to fibrous after being treated with CtsB for 5 h, because the concentration of generated P3 was too low, while obvious nanofibers were observed with the incubation time up to 10 h. For the control peptide P2, there was no obvious conformational change after the treatment of CtsB for 10 h (Figure S7, Supporting Information). Therefore, P1 could be cleaved by CtsB to generate the residue P3[19] (Figure S8, Supporting Information), realizing the nanoparticles-to-nanofibers morphological change. As shown in Figure 2c, the P1 assemblies showed a positive CD signal at 195 nm and negative signals at 210 and 223 nm after incubation with CtsB for 10 h, which suggested the typical fibrous structure,[20] while there was no signal over 200 nm for P1 in the absence of CtsB. Furthermore, wide-angle X-ray scattering (WAXS) was employed for analyzing the molecular arrangement mode (Figure 2e). The WAXS gave two d-spacings (Figure 2f), where the distance between two adjacent strands is 4.6 Å, and 15.1 Å spacing was relevant to two sheets in the bilayers.[21] According to the analysis of CD and WAXS results, a molecular arrangement model was presented in Figure 2g.

Given that CtsB is mainly overexpressed in lysosomes of cancer cells, efficient cellular endocytosis and lysosomal location of P1 are the primary requirement for their catalytic transformation. The location of P1 nanoparticles in CtsB-overexpressed HeLa cells was monitored by confocal laser scanning microscope (CLSM), and as expected, the intensive green fluorescence of GFP from P1 distinctly overlapped with lysotracker labeled with red fluorescence (**Figure 3**a). Furthermore, the location of P3 was tracked upon chemical labeling with the fluorescent dye ATTO 488 (called P3-FL). The green fluorescence from P3-FL could overlap well with the red fluorescence from mitochondria (Figure S9, Supporting Information), showing P1 could act on mitochondria after CtsB digestion. The intracellular morphology transformation of P1 was studied by Bio-TEM, as shown in Figure 3b, the fibrous structures were observed for P1-treated cells, while there were no corresponding structures for P2-treated cells or PBS-treated cells (Figure S10, Supporting Information). This phenomenon demonstrated the formation of nanofibers in cells originated from the transformation of P1 nanoparticles and nanofibers were generated in the cytoplasm. Both SEM and Bio-TEM images of isolated mitochondria prove that the nanofibers can entangle the mitochondria, while the nanoparticles cannot attach to the mitochondria (Figures S11 and S12, Supporting Information).

Furthermore, the cytotoxicity of P1 and P2 to HeLa cells was evaluated after co-incubation with HeLa cells for 48 h, as presented in Figure 3c, P2 was almost no cytotoxic, while P1 induced significant cell death with a low IC_{50} of 15.24 μM, revealing that morphologic transformation could increase the inhibition of HeLa cells by exposing the active site BAK. Similarly, P1 also showed significant cytotoxicity to A375 cancer cells that also overexpressed cathepsin B. In contrast, P1 and P2 showed no toxicity at the same concentration toward the normal cell line of HPF with a low level of cathepsin B expression (Figure S13, Supporting Information). To further study the mechanism of cell death, immunoblot analysis of anti-apoptosis proteins, pro-apoptosis proteins, and apoptosis-related proteins was conducted for HeLa cells treated with 15.24 μM of P1, P2, and PBS, respectively. P1 strongly inhibited Anti-apoptotic Bcl-2 family proteins including Bcl-2, Bcl-xL, and Mcl-1 were inhibited for P1 treated cells

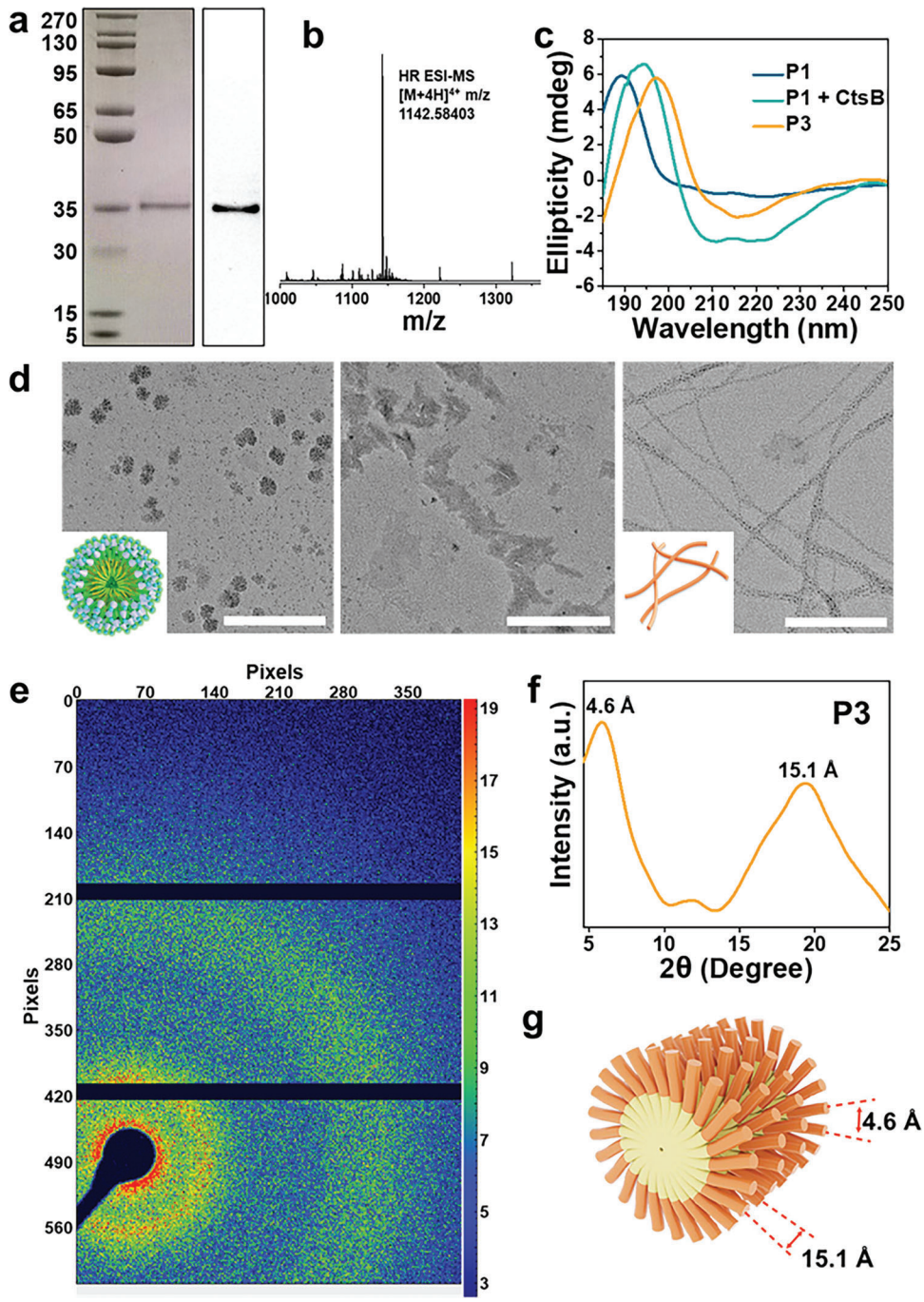

Figure 2. a) SDS-PAGE with a marker range from 5 to 270 kDa and Western blot analysis of the integrity and purity of recombinant protein P1. b) High-resolution LC-MS of P1 incubated with CtsB in an acetate buffer solution (AB, 0.01 M, pH 5.0) for 10 h. c) CD spectra of P1, and P1 treated with CtsB, as well as P3. d) Schematic illustrations of morphology transformation of P1 induced by CtsB, and representative TEM images of P1 and P1 in the presence of CtsB (1.0 μg mL^{-1}, acetate buffer, 0.01 M, pH 5.0) for 5 and 10 h, respectively. Scale bars, 200 nm. e) 2D wide-angle X-ray scattering of P3, and f) the d-spacings of 4.6 and 15.1 Å were attributed to the spacing of the adjacent strands and laminates, respectively. g) The proposed β-sheet molecular arrangement of P3.

(Figure 3d and Figure S14a, Supporting Information), while the expression of apoptotic family proteins Bim, Bad, Bax, and Bak increased (Figure 3e and Figure S14b, Supporting Information). In contrast, the corresponding proteins of these two families were not altered after being treated with P2. Moreover, the level of cytochrome c, cleaved-caspase-9, and cleaved caspase-3 was increased for P1-treated cancer cells compared with that of P2 (Figure 3f and Figure S14c, Supporting Information). Together, these results indicate that P1 induced mitochondria-dependent apoptosis through the Bcl-2 pathway (Figure 3g).[22]

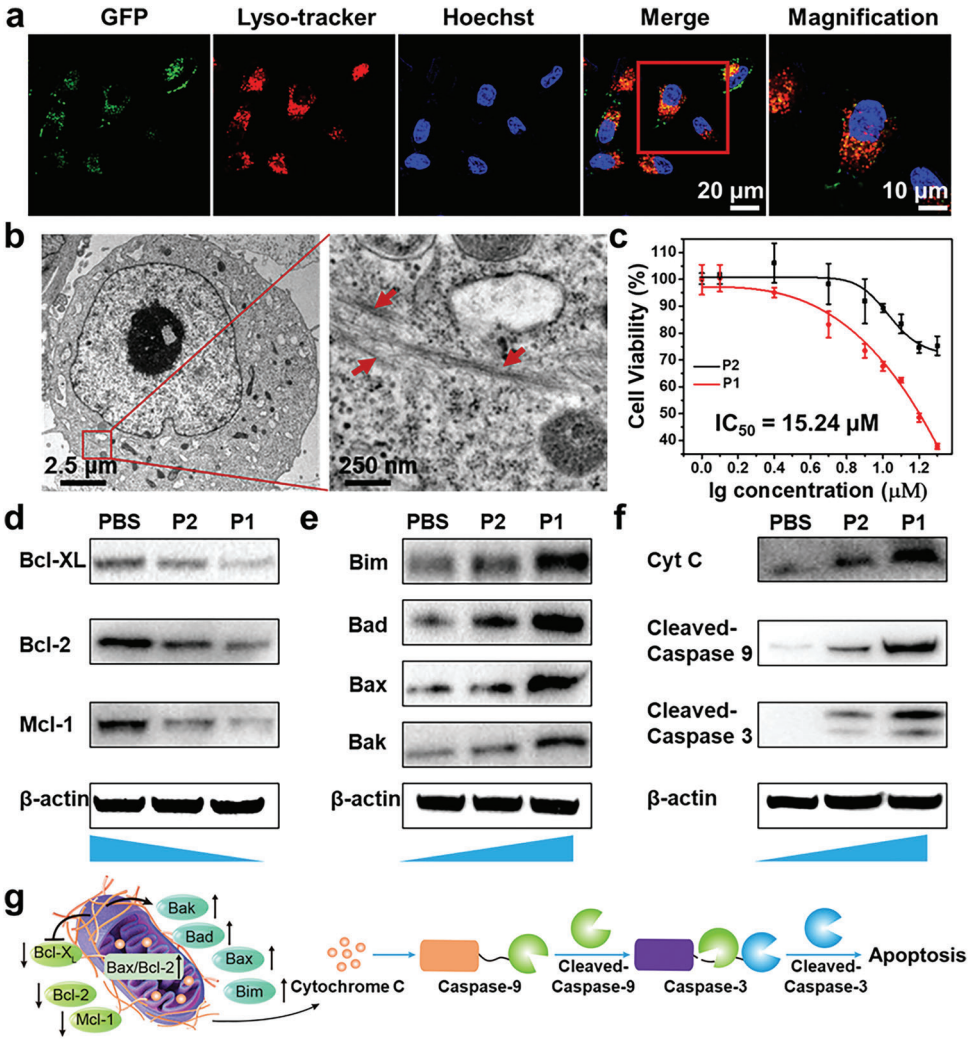

Figure 3. a) CLSM images of HeLa cells treated with P1. b) Bio-TEM images of the ultrathin cell sections of P1. The red arrows indicated the nanofibers. c) Cell viability of P1 and P2 to HeLa cells. Immunoblot analysis of d) anti-apoptosis proteins, e) pro-apoptosis proteins, and f) apoptosis-related proteins in HeLa cells after incubation with PBS, P1, and P2. *β*-actin was analyzed as the internal control. g) Schematic representation of the caspase-dependent apoptosis pathway of the nanofibers acted on the mitochondria.

Living bacteria therapies have been proposed as an alternative approach for the treatment of cancers due to their superior tumor colonizing ability.[23] Here, we constructed a spatiotemporally controllable anticancer system by coating *E. coli* capable of expressing P1 with cationic conjugated polymer (**Figure 4**a). Cationic conjugated polyelectrolytes could be used for coating *E. coli* through electrostatic and hydrophobic interactions.[24] *E. coli* capable of expressing P1 (*E. coli*-[P1]) were coated with a polyfluorene derivative PFP, which could serve as a photosensitizer to generate ROS under white light irradiation.[25] The generated ROS facilitated the fracture of *E. coli* to release the expressed protein P1, which could perform the morphological transformation and induce apoptosis of cancer cells. The CLSM images revealed that almost all the bacteria were effectively labeled by PFP after incubating *E. coli* with PFP for 30 min (Figure 4b). Isothermal titration microcalorimetry and zeta potential measurement were conducted to confirm the interactions of PFP with *E. coli*. (Figure S15, Supporting Information). The initial negative ΔH_{obs} values demonstrated the electrostatic binding of cationic PFP with negatively charged *E. coli*. The ΔH_{obs} values became less exothermic with the titrations of PFP into *E. coli* solutions, and finally reached a platform close to zero, suggesting that the PFP and *E. coli* interaction attains the saturation point. The zeta potential of separated *E. coli* was -44.5 ± 0.2 mV, and the zeta potential of *E. coli* gradually exhibited a positive shift after incubation with different concentrations of cationic PFP. These results also indicated that PFP would bind to the surface of *E. coli* through electrostatic interaction.

The ability of PFP to damage the bacterial membrane was assessed by live/dead co-staining assays. Most *E. coli* remained alive in the dark after being treated with different concentrations of PFP, indicating the good biocompatibility of PFP. Upon white light irradiation (50 mW cm^{-2}) for 30 min, most *E. coli* were dead because of the generated ROS from PFP (Figure S16, Supporting Information), which suggested that 40 μM PFP could cause a high level of bacterial membrane destruction. SEM

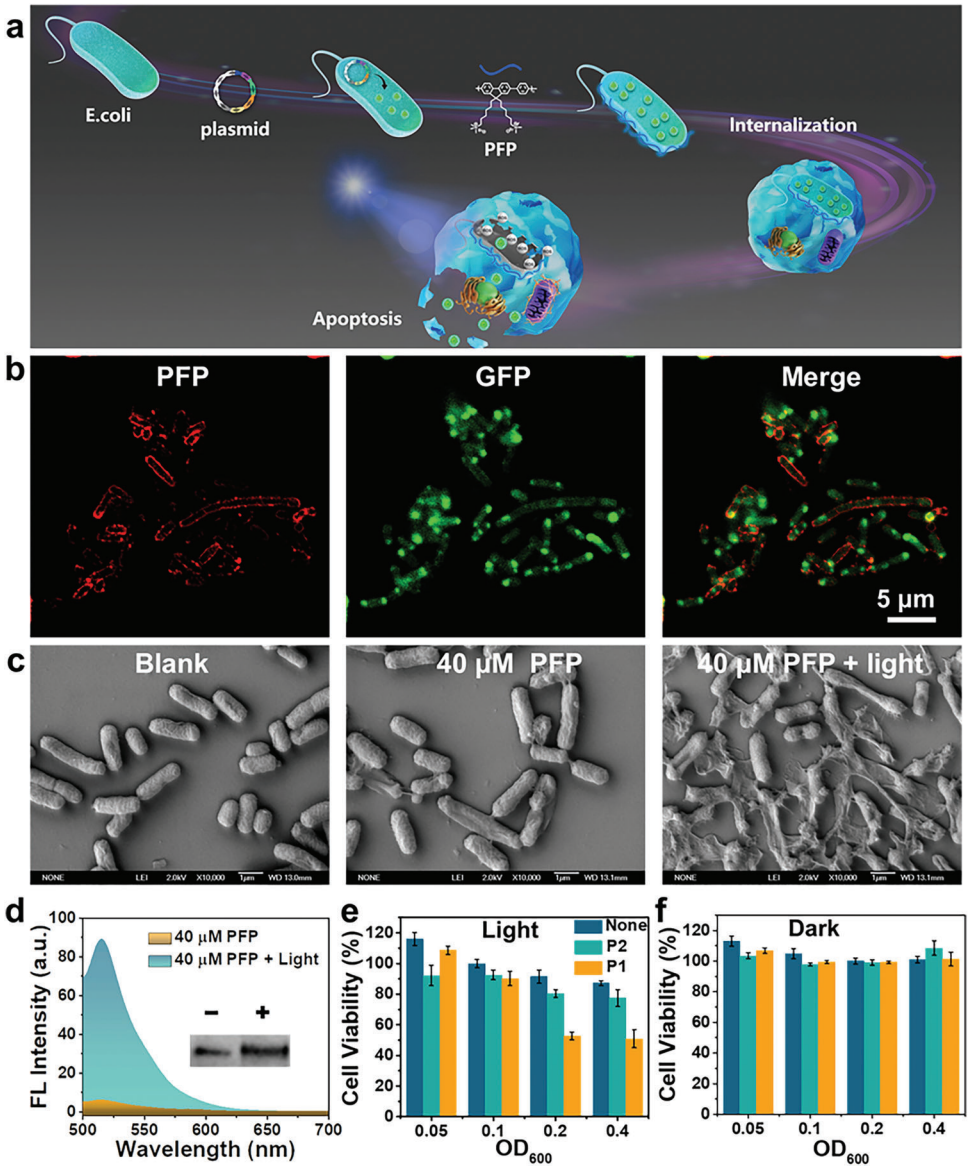

Figure 4. a) Schematic diagram of cationic PFP-coated live bacteria for controlled intracellular release of transformable peptides with light manipulation. b) CLSM of PFP-coated *E. coli*-[P1] (40 μM PFP). c) SEM images of PFP-coated *E. coli*-[P1] with and without light irradiation. d) The fluorescence spectra of the released P1 from *E. coli* induced with and without light irradiation. Insets: western blot analysis of the released P1 from *E. coli* with and without light irradiation. Cell viability analysis of PFP-coated *E. coli* against HeLa cells with e) and without f) white light irradiation.

was then utilized to get an intuitive state of the bacterial membranes treated by PFP. As shown in Figure 4c, *E. coli* alone possesses clear edges and smooth outer surfaces, and the outer surfaces remained intact but became rough after coating with PFP. Under light irradiation, the collapse, rupture, and fusion of *E. coli* were greatly enhanced, and the shape of *E. coli* was hardly recognized. The damage of bacterial membrane favors the persistent release of various intracellular contents including P1. After centrifuging the bacterial solutions, the supernatant was collected and a sharply increased fluorescence intensity of GFP was observed (Figure 4d). The bacterial fragments and proteins were observed by TEM (Figure S17, Supporting Information). The successful release of P1 from *E. coli* in the supernatant was also confirmed by western blotting assay (inset in Figure 4d).

The cellular uptake of PFP-coated *E. coli*-[P1] by HeLa cells was observed by CLSM. Green fluorescence from GFP overlapped well with blue signals of PFP in the cytoplasm of HeLa cells, which indicated that most bacteria were tightly covered by the PFP (Figure S18, Supporting Information). The previously intact *E. coli* disintegrated upon irradiation with white light (Figure S19, Supporting Information). As depicted in Figure 4e, the killing efficiency of expressed P1 increased dramatically and the highest killing efficiency reached over 50% after light irradiation, while there was no obvious cytotoxicity for *E. coli* expressed P2 even with relatively high bacterial concentration. For the dark groups,

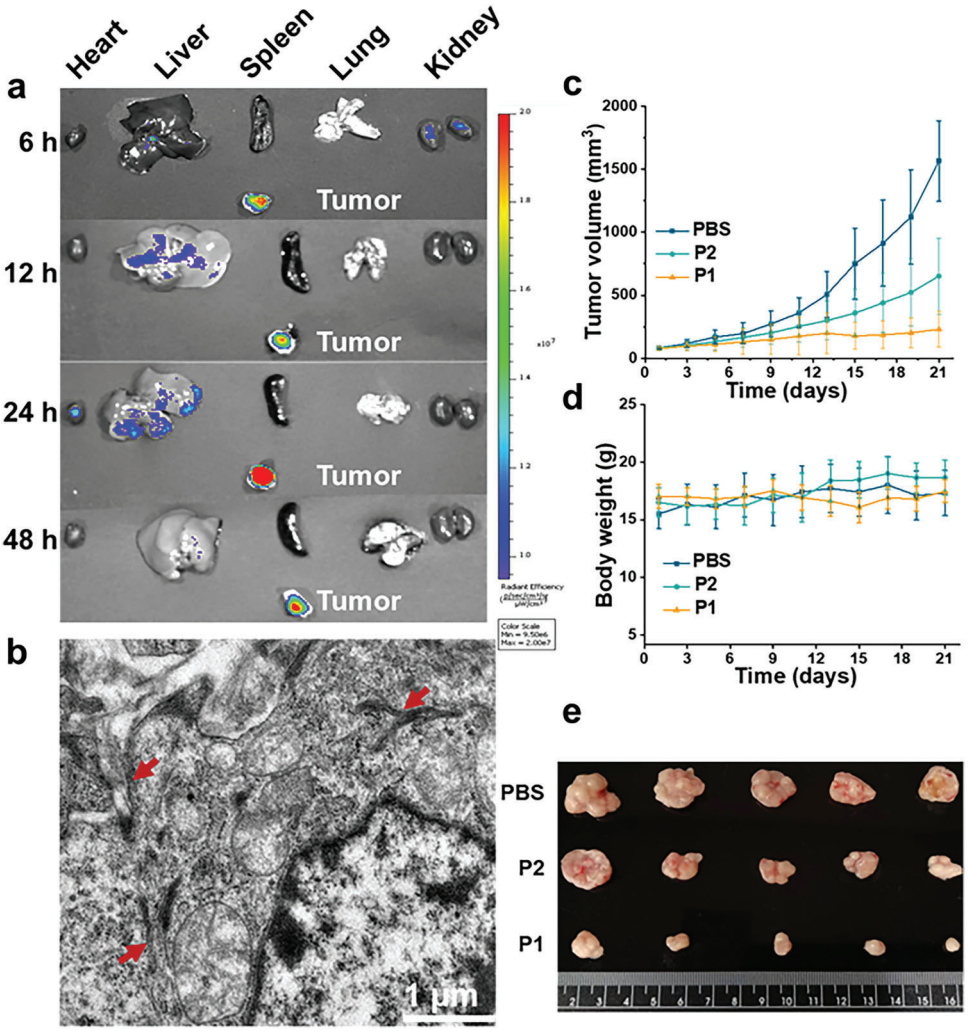

Figure 5. a) Time-dependent ex vivo fluorescence of tumor tissues and major organs in P1 treated mice at 6, 12, 24, and 48 h after single dose i.v. administration. b) Bio-TEM images of distribution in tumor tissue and in situ fibrillar transformation of P1 at 48 h post-injection. c) Relative tumor volume and d) weight change of mice in the subcutaneous tumor model during the therapy for 21 days ($n = 5$ per group). e) Representative photos of mice tumors after 21 days of treatments.

cells were all basically unaffected for 48 and 72 h, which verified that the PFP-coated bacteria were biocompatible (Figure 4f and Figure S20, Supporting Information). These results demonstrated that the release of active drugs from living bacteria was successfully regulated in time through light manipulation in a non-invasive and remote-control manner.

The effect of morphology transformation on tumor accumulation and therapeutic efficacy were evaluated in vivo with cervical tumor-bearing female BALB/c nude mice models. After being administered with P1, P2, or PBS, the tumor and major organs were collected for ex vivo fluorescent imaging at 6, 12, 24, and 48 h, respectively (**Figure 5**a and Figure S21, Supporting Information). The highest fluorescence intensity in tumor tissue was observed at 24 h and began to decline after 24 h. In contrast, there was negligible signal in major organs during the whole process, which proved that the biosynthesized peptides exhibited good tumor-targeting ability due to the moiety of T22. Bio-TEM was utilized to study the morphological transformation of P1 on excised tumor tissues after 48 h intravenous (i.v.) administration. As illustrated in Figure 5b, the fibrous structures were observed in tumor slices for P1 treated mice, while not for P2 and PBS groups (Figure S22, Supporting Information). To evaluate therapeutic efficiency, P1 was injected consecutively six times q.o.d. in the tail vein and continuously observed for 21 days, as displayed in Figure S23, Supporting Information. P1 exhibited more significant tumor inhibition efficacy than other groups and tumor volume of P1-treated mice gradually shrank (Figure 5c,e), which could be attributed to the exposure of the active sites after digestion. Compared to the PBS group, a relatively poor response was obtained for negative control P2-treated mice, where cleavable sites of the enzyme were not introduced.

There is no obvious body weight loss for all mice groups (Figure 5d). Hematoxylin–eosin (H&E) staining of the major organs did not display obvious pathological changes at the treatment dose, which proved that the transformable P1 treatment for tumor ablation was biocompatible (Figure S24, Supporting

Information). Next, both H&E staining and TdT-mediated dUTP nick end labeling assay exhibited a large amount of necrosis in the tumor tissues after being treated with P1 (Figure S25a,b,d, Supporting Information). Immunofluorescence staining was conducted to further confirm the activation of the endogenous apoptosis pathway of P1. As shown in Figure S25c,f, Supporting Information, 81% cleaved-caspase-3 was observed in P1 treated group, which was higher than that for the P2 treatment. In contrast, the expression level of Ki-67 in tumor tissues was found to be significantly reduced after being treated with P1, in comparison with the P2 treatment group (Figure S25e, Supporting Information). All these results demonstrated that P1 promoted apoptosis of cancer cells.

3. Conclusion

In summary, we introduced biosynthesized PBMs capable of intracellular morphological transformation that can efficiently induce tumor cell apoptosis. The recombinant protein P1 was composed of H6-T22-GFP-BAK-KLVFF-RGD integrated with multiple functions. GFP and BAK-KLVFF were released by CtsB digestion, leading to the transformation from nanoparticles to nanofibers in situ, which could expose the BAK active sites. BAK could bind to mitochondria and change the mitochondrial permeability, which further promoted apoptosis of cancer cells. Extensive ex vivo and in vivo experiments demonstrated that this enzyme-catalytic transformation strategy based on in situ self-assembly could effectively suppress tumor growth. Moreover, a photo-responsive protein-releasing system was established by introducing PFP as the photosensitizer. Taking the PFP-coated bacteria as the carriers, the cargo could be released in a photo-controlled manner. Consequently, the morphology transformation of recombinant protein was initiated to induce cell apoptosis in situ. These characteristics of biosynthesized PBMs will facilitate their further use in the treatment of cancers. Moreover, it is worth mentioning that the proposed biomaterials are proliferative and evolvable living materials. They could contribute to better therapeutic performance and advance more specific biochemical applications when genetically integrated with more functions. For example, the biosynthesized PBMs could change the active site BAK to immune-active proteins such as the anti-PDL1 sequence to improve the immunotherapeutic effect on tumors.[15] In the future, multimodal therapy will be developed on the basis of PBMs to efficiently improve the therapeutic effect on tumors.

Supporting Information

Supporting Information is available from the Wiley Online Library or from the author.

Acknowledgements

This work was supported by the National Natural Science Foundation of China (Nos. 22021002, 22020102005, 22022705, and 22074150) and the CAS-Croucher Funding Scheme for Joint Laboratories.

Conflict of Interest

The authors declare no conflict of interest.

Data Availability Statement

Research data are not shared.

Keywords

biosynthesis, living materials, nanofibers, self-assembled proteins, transformation

Received: April 11, 2023
Revised: June 12, 2023
Published online:

[1] a) A. Chilkoti, M. R. Dreher, D. E. Meyer, *Adv. Drug Delivery Rev.* **2002**, *54*, 1093; b) S. A. Maskarinec, D. A. Tirrell, *Curr. Opin. Biotechnol.* **2005**, *16*, 422; c) M. Haider, Z. Megeed, H. Ghandehari, *J. Controlled Release* **2004**, *95*, 1.
[2] a) R. Langer, D. A. Tirrell, *Nature* **2004**, *428*, 487; b) G. B. Qi, Y. J. Gao, L. Wang, H. Wang, *Adv. Mater.* **2018**, *30*, 1703444.
[3] a) G. M. Lynn, C. Sedlik, F. Baharom, Y. Zhu, R. A. Ramirez-Valdez, V. L. Coble, K. Tobin, S. R. Nichols, Y. Itzkowitz, N. Zaidi, J. M. Gammon, N. J. Blobel, J. Denizeau, P. de la Rochere, B. J. Francica, B. Decker, M. Maciejewski, J. Cheung, H. Yamane, M. G. Smelkinson, J. R. Francica, R. Laga, J. D. Bernstock, L. W. Seymour, C. G. Drake, C. M. Jewell, O. Lantz, E. Piaggio, A. S. Ishizuka, R. A. Seder, *Nat. Biotechnol.* **2020**, *38*, 320; b) H. W. An, L. L. Li, Y. Wang, Z. Wang, D. Hou, Y. X. Lin, S. L. Qiao, M. D. Wang, C. Yang, Y. Cong, Y. Ma, X. X. Zhao, Q. Cai, W. T. Chen, C. Q. Lu, W. Xu, H. Wang, Y. Zhao, *Nat. Commun.* **2019**, *10*, 4861; c) T. Kunitake, *Angew. Chem., Int. Ed.* **1992**, *31*, 709.
[4] H. He, S. Liu, D. Wu, B. Xu, *Angew. Chem., Int. Ed.* **2020**, *59*, 16445.
[5] a) D. B. Cheng, D. Wang, Y. J. Gao, L. Wang, Z. Y. Qiao, H. Wang, *J. Am. Chem. Soc.* **2019**, *141*, 4406; b) Y. Di, E. Zhang, Z. Yang, Q. Shen, X. Fu, G. Song, C. Zhu, H. Bai, Y. Huang, F. Lv, L. Liu, S. Wang, *Angew. Chem., Int. Ed.* **2022**, *61*, e202116457.
[6] P.-P. Yang, Q. Luo, G.-B. Qi, Y.-J. Gao, B.-N. Li, J.-P. Zhang, L. Wang, H. Wang, *Adv. Mater.* **2017**, *29*, 1605869.
[7] a) L. Zhang, Y. Liu, H. Huang, H. Xie, B. Zhang, W. Xia, B. Guo, *Adv. Drug Delivery Rev.* **2022**, *190*, 114536; b) T. Senthilkumar, L. Zhou, Q. Gu, L. Liu, F. Lv, S. Wang, *Angew. Chem., Int. Ed.* **2018**, *57*, 13114; c) S. Roy, N. Bag, S. Bardhan, I. Hasan, B. Guo, *Adv. Drug Delivery Rev.* **2023**, *197*, 114821.
[8] D. Mozhdehi, K. M. Luginbuhl, J. R. Simon, M. Dzuricky, R. Berger, H. S. Varol, F. C. Huang, K. L. Buehne, N. R. Mayne, I. Weitzhandler, M. Bonn, S. H. Parekh, A. Chilkoti, *Nat. Chem.* **2018**, *10*, 496.
[9] a) X. Lv, C. Zhang, Q. Shuaizhen, R. Yu, Y. Zheng, *Biomed. Pharmacother.* **2020**, *128*, 110236; b) X. Fu, Y. Huang, H. Zhao, E. Zhang, Q. Shen, Y. Di, F. Lv, L. Liu, S. Wang, *Adv. Mater.* **2021**, *33*, 2102570.
[10] C. Pan, J. Wu, S. Qing, X. Zhang, L. Zhang, H. Yue, M. Zeng, B. Wang, Z. Yuan, Y. Qiu, H. Ye, D. Wang, X. Liu, P. Sun, B. Liu, E. Feng, X. Gao, L. Zhu, W. Wei, G. Ma, H. Wang, *Adv. Mater.* **2020**, *32*, 2002940.
[11] a) L. Sánchez-García, N. Serna, P. Álamo, R. Sala, M. V. Céspedes, M. Roldan, A. Sánchez-Chardi, U. Unzueta, I. Casanova, R. Mangues, E. Vázquez, A. Villaverde, *J. Controlled Release* **2018**, *274*, 81; b) C. de la Torre, I. Casanova, G. Acosta, C. Coll, M. J. Moreno, F. Albericio, E. Aznar, R. Mangues, M. Royo, F. Sancenón, R. Martínez-Máñez, *Adv. Funct. Mater.* **2015**, *25*, 687; c) R. Díaz, V. Pallarès, O. Cano-Garrido, N. Serna, L. Sánchez-García, A. Falgàs, M. Pesarrodona, U. Unzueta, A. Sánchez-Chardi, J. M. Sánchez, I. Casanova, E. Vázquez, R. Mangues, A. Villaverde, *Small* **2018**, *14*, 1800665.
[12] a) U. Unzueta, M. V. Cespedes, N. Ferrer-Miralles, I. Casanova, J. Cedano, J. L. Corchero, J. Domingo-Espin, A. Villaverde, R. Mangues, E. Vazquez, *Int. J. Nanomed.* **2012**, *7*, 4533; b) L. Sanchez-Garcia, N.

Serna, P. Alamo, R. Sala, M. V. Cespedes, M. Roldan, A. Sanchez-Chardi, U. Unzueta, I. Casanova, R. Mangues, E. Vazquez, A. Villaverde, *J. Controlled Release* **2018**, *274*, 81.
[13] A. Pena-Blanco, A. J. Garcia-Saez, *FEBS J.* **2018**, *285*, 416.
[14] a) K. Cosentino, A. J. García-Sáez, *Trends Cell Biol.* **2017**, *27*, 266; b) R. Salvador-Gallego, M. Mund, K. Cosentino, J. Schneider, J. Unsay, U. Schraermeyer, J. Engelhardt, J. Ries, A. J. García-Sáez, *EMBO J.* **2016**, *35*, 389; c) M. P. A. Luna-Vargas, J. E. Chipuk, *Trends Cell Biol.* **2016**, *26*, 906; d) E. P. Holinger, T. Chittenden, R. J. Lutz, *J. Biol. Chem.* **1999**, *274*, 13298.
[15] J. Dai, J. J. Hu, X. Dong, B. Chen, X. Dong, R. Liu, F. Xia, X. Lou, *Angew. Chem., Int. Ed.* **2022**, *61*, e202117798.
[16] a) X. Ai, C. J. H. Ho, J. Aw, A. B. E. Attia, J. Mu, Y. Wang, X. Wang, Y. Wang, X. Liu, H. Chen, M. Gao, X. Chen, E. K. L. Yeow, G. Liu, M. Olivo, B. Xing, *Nat. Commun.* **2016**, *7*, 10432; b) L. Hu, Y. Li, X. Lin, Y. Huo, H. Zhang, H. Wang, *Angew. Chem., Int. Ed.* **2021**, *60*, 21807.
[17] a) J. Yang, R. Yan, A. Roy, D. Xu, J. Poisson, Y. Zhang, *Nat. Methods* **2015**, *12*, 7; b) J. Yang, Y. Zhang, *Nucleic Acids Res.* **2015**, *43*, W174.
[18] M. C. Huber, A. Schreiber, P. von Olshausen, B. R. Varga, O. Kretz, B. Joch, S. Barnert, R. Schubert, S. Eimer, P. Kele, S. M. Schiller, *Nat. Mater.* **2015**, *14*, 125.
[19] Y.-J. Cheng, G.-F. Luo, J.-Y. Zhu, X.-D. Xu, X. Zeng, D.-B. Cheng, Y.-M. Li, Y. Wu, X.-Z. Zhang, R.-X. Zhuo, F. He, *ACS Appl. Mater. Interfaces* **2015**, *7*, 9078.
[20] a) J. Zhan, Y. Cai, S. Ji, S. He, Y. Cao, D. Ding, L. Wang, Z. Yang, *ACS Appl. Mater. Interfaces* **2017**, *9*, 10012; b) H. Sun, J. Liu, S. Li, L. Zhou, J. Wang, L. Liu, F. Lv, Q. Gu, B. Hu, Y. Ma, S. Wang, *Angew. Chem., Int. Ed.* **2019**, *58*, 5988.
[21] a) B. H. San, J. Hwang, S. Sampath, Y. Li, L. L. Bennink, S. M. Yu, *J. Am. Chem. Soc.* **2017**, *139*, 16640; b) M. Kastler, J. Schmidt, W. Pisula, D. Sebastiani, K. Müllen, *J. Am. Chem. Soc.* **2006**, *128*, 9526.
[22] a) L. Liu, Z. Huang, J. Chen, J. Wang, S. Wang, *J. Cell. Biochem.* **2018**, *119*, 6633; b) C. P. Dillon, D. R. Green, *Adv. Exp. Med. Biol.* **2016**, *930*, 1.
[23] a) Y. A. Yu, S. Shabahang, T. M. Timiryasova, Q. Zhang, R. Beltz, I. Gentschev, W. Goebel, A. A. Szalay, *Nat. Biotechnol.* **2004**, *22*, 313; b) J.-J. Min, V. H. Nguyen, H.-J. Kim, Y. Hong, H. E. Choy, *Nat. Protoc.* **2008**, *3*, 629; c) Y. Yue, J. Xu, Y. Li, K. Cheng, Q. Feng, X. Ma, N. Ma, T. Zhang, X. Wang, X. Zhao, G. Nie, *Nat. Biomed. Eng.* **2022**, *6*, 898.
[24] a) C. Zhu, Q. Yang, F. Lv, L. Liu, S. Wang, *Adv. Mater.* **2013**, *25*, 1203; b) H. Bai, H. Chen, R. Hu, M. Li, F. Lv, L. Liu, S. Wang, *ACS Appl. Mater. Interfaces* **2016**, *8*, 31550.
[25] a) C. Zhu, L. Liu, Q. Yang, F. Lv, S. Wang, *Chem. Rev.* **2012**, *112*, 4687; b) X. Duan, L. Liu, X. Feng, S. Wang, *Adv. Mater.* **2010**, *22*, 1602.